Talanta 210 (2020) 120671

Contents lists available at ScienceDirect

Talanta

journal homepage: www.elsevier.com/locate/talanta

Size controllable, pH triggered reduction of bovine serum albumin and its adsorption behavior with SnO_2/SnS_2 quantum dots for biosensing application

Dhananjayan Nathiya[a], Karuppasamy Gurunathan[b], Jeyaraj Wilson[a,*]

[a] Department of Bioelectronics and Biosensors, Alagappa University, Karaikudi, 630 003, India
[b] Department of Nanoscience and Technology, Alagappa University, Karaikudi, 630 003, India

ARTICLE INFO

Keywords:
Bovine serum albumin
Tin sulfide
Hybrid composite
Melatonin
Biosensor

ABSTRACT

The pH dependent size control of Bovine Serum Albumin (BSA) and its biosensing potential with Tin Oxide and Tin Sulfide Quantum Dots (SnO_2/SnS_2 QDs) is reported. The role of disulfide bond cleavage in BSA at acidic and circumneutral pH conditions (3 and 7.2) with sodium borohydride as reducing agent, makes changes in its stability, prone to aggregation and microcapsule formation respectively. Here, the structural reduction in BSA (r-BSA2) at pH 7.2 probed more –OH groups eventually creating adhesive surfaces for SnO_2/SnS_2 QDs due to electrostatic and hydrophobic forces, thus avoids the aggregation of SnO_2/SnS_2 QDs in composite formation. The accumulation of more active sites in SnO_2/SnS_2 QDs decorated r-BSA2 (SnO_2/SnS_2@r-BSA2) nanobiocomposite favored suitable orientation for Melatonin (Mel) detection. The designed SnO_2/SnS_2@r-BSA2 nanobiocomposite over the screen printing electrode exhibited electrochemical detection capabilities for the selective and sensitive recognition of Mel in the linear range of 0.2–1000 μM with a lower detection limit of 16 nM. Additionally, the fabricated biosensor was successfully validated for the determination of Mel in real samples.

1. Introduction

Bovine Serum Albumin (BSA), a heart shaped globular protein, composed of 583 amino acids in a single polypeptide chain with disulfide linkages as well as active functional groups such as carboxyl and thiol groups, plays a major role because of their intensive research activities in recent years. Since the protein model is in high similarity of 76% sequence homology with human serum albumin, widely employed in biomedical applications [1–3]. Interestingly, the critical influencing factors of BSA such as interaction with other biomaterials/nanomaterials, identification of most important residues, structural changes with varying pH and temperature conditions developed interest to analyze their electrochemical behavior for various applications [4,5].

Firstly, the insight study on structural changes in BSA at different pH condition remained to be challenge and its application in biomedical field is on trend now owing to its various physiological functions. At acidic pH range (< 3.5), an extended form of structure due to the disulfide bond integrity and aggregation of BSA result to fibril formation. In contrast on increasing pH from neutral (> 7.0), exhibit normal form and some of the disulfide bonds in protein can be cleavable by reducing environment and found to produce micro and nanocapsule formation, whereas all the disulfide bonds are protected between acidic and neutral (pH 4–7) [5,6]. However, the understanding of disulfide bond cleavage and structural deformation in BSA at acidic and neutral pH conditions remains to be a challenge. Secondly, BSA also found to undergo structural changes on adsorption by providing stabilized platform due to the contribution of electrostatic and hydrophobic interactions [7,8]. The reported materials that initiated the structural changes in BSA upon adsorption are ellagitannin [9], chitosan [10], tellurium [11], dextran [12], polypyrrole [13], etc. It is well observed from these reports that the structural changes of protein with suitable performances in the composite pave a novel platform to designing new innovative hybrid biomaterials for biosensing application. The adsorption and folding capacity of BSA with other biomolecule/nanomaterials depends on the charging nature which also gets varied by increasing pH [10,14]. At pH 7, negative nature of BSA bind electrostatically with another negatively charged metal nanoparticle due to the presence of several positively charged lysine amino acid in that [15,16]. In this study, we used sodium borohydride, a well-known strong reducing agent, to investigate di-sulfide bond cleavage in protein that leads to structural changes at pH3 and pH7.2. The change in secondary structure of BSA upon adsorption with nanomaterial and its

* Corresponding author.
E-mail address: wilson.j2008@yahoo.com (J. Wilson).

https://doi.org/10.1016/j.talanta.2019.120671
Received 17 August 2019; Received in revised form 6 December 2019; Accepted 22 December 2019
Available online 23 December 2019
0039-9140/

enhanced steric performance is also discussed in this paper.

Quantum dots (QDs) are extensively used for biomedical application due to its miniaturized structure, biocompatibility, narrow band emission and versatile surface modification [17]. It also reported to have covalent bonding ability with biomolecule and also promote direct electron transfer between biomolecule and electrode surface [18,19]. However to the best of our knowledge no significant efforts have been made for the investigation of metal oxide/sulfide based QDs in biosensor yet. In this paper, we report the Tin oxide sulfide (SnO_2) and Tin disulfide (SnS_2) QDs decorated BSA and utilize in effective biomolecule detection. In recent years, SnS_2 have attracted tremendous attention due to their layered crystal phase, narrow band gap (2.2 eV), good stability in acid and neutral aqueous solutions, and thermal stability. Benefitting from free of dangling bonds, low-price, less surface trap, and lower toxicity contributed as a promising material in various fields, including dye-sensitized solar cells [20], photocatalytic hydrogen generation [21], lithium-ion batteries [22], etc. However, the SnS_2 sheet like structure, limited its potential application in biosensor field due to its poor electron transportation. The coupling of two different semiconductors reported to execute high photocatalytic performance as compared to single semiconductors [23]. As mentioned above, a lot of attempts have been made to improve the electro chemical behavior of SnS_2 for biosensing applications through morphology control, doping process, using carbon based materials [24,25], etc. Herein we propose another effective way of using SnS_2 QDs with SnO_2 QDs and made a composite with protein for enhancing the electron transfer process thus to provide a stable structure. So, the construction of heterostructure based on SnO_2/SnS QDs decorated with reduced BSA composite having well-matched band structure which is a highly desired character for the fabrication of novel biosensor.

Melatonin (Mel), a hormone secreted by pineal gland in mammalian brain, possesses antioxidant property and helps to regulate sleep-wake cycle and other hormone production. The deficiency of Mel leads to several neurological disorders and risk of cancer. Mel also regulates antioxidant enzymes in human body and act as a very effective free radical scavenger that protect tissues from the reactive oxygen and nitrogen species [26,27]. Therefore the daily intake of Mel (0.1–1 mg) has been prescribed for the regulation of neurological stability. Usually Mel is rich in food items such as vegetables and fruits and thus detection of Mel content can quantify the food products [28]. And also its quantification in human fluids can lead to early diagnosis of many physiological and behavioral disorders. Several analytical techniques such as HPLC [29], spectrofluorimetric [30], colorimetric [31], and electrochemical methods [25] have been reported for the detection of Mel. Among these, electrochemical method is reported to be simple, fast and high selectivity towards the selective determination of Mel.

In this paper, we present the structural modification in BSA at different pH conditions (3 and 7.2) and its steric behavior with SnO_2/SnS QDs was utilized as biosensing platform. Importantly, the prepared nanobiocomposite exhibit selective determination towards Mel with very low detection limit (S/N = 3σ) and wide linear range of 16 nM and 0.2–1000 μM respectively. The fabricated electrode also tested in human urine samples and recovered the significant concentration of Mel supporting the real time application of the proposed biosensor.

2. Experimental section

2.1. Materials

All chemicals were analytical grade and used without further purification. Bovine Serum Albumin, Sodium Borohydride ($NaBH_4$), acetone, Tin(IV) chloride ($SnCl_4.5H_2O$, 99%), thiourea (CH_4N_2S), Melatonin were purchased from Himedia, Mumbai. 10 mM of Mel solution was freshly prepared in prior to its use. 0.1 M Phosphate Buffer solution (PBS) was prepared as supporting electrolyte and adjusted to pH7 using NaOH solution. For aqueous solutions, de-ionized (DI) water was used. Experiments were conducted at room temperature (25 °C).

2.2. Electrode preparation and modification

2.2.1. Preparation of BSA microcapsules at different pH conditions

The structural and disulfide bond reduction in BSA was carried out by the addition of strong reducing agent $NaBH_4$ at different pH (3 and 7.2) conditions. In Brief, 0.5 g of BSA was dissolved in 50 mL of DI water by stirring and the solution mixture was maintained at pH7.2. In that 5% $NaBH_4$ (0.2 g in 5 mL DI water) was added for the reduction of disulfide bonds in BSA and stirred for 3 h. Then the pH value was increased from circumneutral (pH7.2) to basic (pH 8.9) and thus resulting reduction in di-sulfide bonds eventually provide reduced BSA structure. By mixing acetone with sample solution in the ratio of 3:1 the modified protein was separated and dried by lyophilizer and the final product named as r-BSA2. In same way, the pH maintained in process was adjusted to 3 by the addition of HCl and then reduced and the product obtained named as r-BSA1. Thus the reduction in BSA creates more –OH and –COOH groups in BSA enabling more electrocatalytic oxidation with –NH group in Mel which acts as a steric platform for SnS QDs.

2.2.2. Preparation of SnO_2/SnS_2 Quantum Dots

SnO_2/SnS_2 QDs were prepared via simple hydrothermal method using $SnCl_4.5H_2O$ and thiourea as tin and sulfur sources respectively. Briefly, 15 mM of $SnCl_4.5H_2O$ (0.26 g) and 60 mM of CH_4N_2S (0.22 g) were stirred and dissolved in 50 mL DI water for 30 min. The mixture solution was then transferred to 80 mL Teflon lined autoclave and heated in oven at 160 °C for 24 h and then cooled to room temperature. The obtained black colour product was washed several times using DI water, ethanol and then dried at 50 °C for 5 h. The possible reaction process responsible for the pH variations of solution mixture and subsequent formation of SnO_2/SnS_2 QDs are as follows:

$$SnCl_4.5H_2O \xrightarrow{\text{Dissolution in } H_2O} Sn^{4+} + 4Cl^- + 5H^+ + 5OH^- \quad (\text{pH } 1.1) \tag{1}$$

$$Sn^{4+} + 5H^+ + 5OH^- + (NH_2)_2C{=}S \xrightarrow[160^{\circ}C]{\text{Hydrolysis}} SnO_2 + SnS_2 + CO + 2NH_4OH + 4H^+ \tag{2}$$

$$2NH_4OH + 4H^+ + 4Cl^- \rightarrow NH_4Cl + 2HCl + 2H_2O \quad (\text{pH } 1.8) \tag{3}$$

2.2.3. Preparation of SnO_2/SnS_2@r-BSA2 modified SPE

For the selection of appropriate composite proportion, different weight ratio of SnO_2/SnS_2 QDs and r-BSA2 was examined in selective sensing of 200 μM of Mel using Cyclic Voltammetry (CV) technique and it is observed that the ratio (1:1) has shown higher oxidation peak which is optimized for the present work (Fig. S1). For electrode modification, SnO_2/SnS_2 QDs decorated r-BSA2 (SnO_2/SnS_2@r-BSA2) mixture solution (5 mg of SnO_2/SnS_2 QDs, 5 mg of r-BSA2 in 1 mL DI water) was prepared by stirring and kept in ultrasonication for 15 min and 6 h respectively. Then, 10 μL of dispersed SnO_2/SnS_2@r-BSA2 aqueous solution was drop casted onto the SPE and allowed to dry at room temperature for 2 h. For comparison purposes, SnO_2/SnS_2 QDs, BSA, r-BSA1 and r-BSA2 were also prepared by similar method.

2.3. Characterization

The electrochemical behavior of prepared samples were analyzed at room temperature, on an CHI6055D electrochemical workstation (Austin, USA), by a Three-Screen Printed Electrode (SPE), which integrates a three-electrode system based on carbon as counter electrode, working electrodes of 3 mm diameter and a silver reference electrode (TE100, Austin, USA). The electrochemical reaction was carried out in PBS at pH 7. The SEM images for SnO_2/SnS_2 QDs, r-BSA1, r-BSA2, and SnO_2/SnS_2@r-BSA2 nanobiocomposite were obtained using Zeiss

operating at 21.00 kV. The energy-dispersive X-ray spectroscopy (ULTRA 55, Zeiss, Germany) was analyzed for SnO_2/SnS_2 QDs and r-BSA2 samples. The TEM images for prepared samples were obtained using Tecnai G2 (F30) High resolution Transmission electron microscope. X-ray photoelectron spectroscopic studies were performed using an AXIS ULTRA(AXIS 165, Kratos, United Kingdom) spectrometer with monochromatic Al Ka (1486.6 eV) radiation. The XRD patterns were obtained using Bruker Germany D8 advance instrument (λ = 1.5418 Å) operated at 30 mA, 40 kV and using Cu kα radiation. The Raman spectrum was obtained using an imaging spectrograph (model STR500 mm focal length) laser Raman spectrometer (SEKI Japan). Fourier Transform Infrared Spectroscopy (FT-IR) was carried out on a Thermo Nicolet 200 FTIR spectrometer with a wavelength ranges from 4000 to 400 cm^{-1}. The UV–vis absorption spectra of aqueous solutions of the samples were recorded (ALS-SEC2000, Biologic, France) in the wavelength 200–800 nm at room temperature. The samples were further characterized by Vibrating sample magnetometer (VSM, cryogenic, UK).

3. Results and discussion

3.1. Material characterization

Fig. 1 shows the XRD patterns of BSA, r-BSA1, r-BSA2, SnO_2/SnS_2 QDs and SnO_2/SnS_2@r-BSA2 samples. In that, compared to BSA, the structurally reduced form of r-BSA1 and r-BSA2 has significant changes in crystalline structure with high angle peaks at 2θ of 15.68, 15.65, 18.39, 20.28, 22.70, 23.81, 35.11° and increase in intensity results in improved crystalline structure signifying the structural modification. XRD peak of 'd' in Fig. 1A indexed the mixture formation of tetragonal phase SnO_2 (JCPDS card no. 41–1445), and hexagonal phase SnS_2 QDs (JCPDS card no. 89–2358). The broadened peak of SnO_2 suggests that the crystalline size of the QDs is very small [32]. In this, we speculated that the formation of small proportion of SnS_2 as compared to SnO_2 and evidenced in further characterization. In peak 'e' the presence of individual peaks and increase in intensity attributed to strong adsorption of SnO_2/SnS_2 QDs on the surface of r-BSA2. Thus, the XRD results suggested the successful electrosteric interaction of SnO_2/SnS_2@r-BSA2 responsible for the enhanced crystalline behavior.

FT-IR spectroscopy was performed over the samples to further confirm structural modification in BSA and its strong interaction with SnO_2/SnS_2. The recorded spectra for BSA, r-BSA1, r-BSA2, SnO_2/SnS_2 QDs and SnO_2/SnS_2@r-BSA2 are presented in Fig. 1B. In curve 'd' the strong peaks observed at 550 cm^{-1} and 652 cm^{-1} represents the stretching vibrations of Sn–S and Sn–O bands [33,34]. The main characteristic peaks for BSA are observed at 1660 cm^{-1} (C═O stretching) and 1524 cm^{-1} (N–H bending and C–N stretching) corresponding to protein amide I and amide II bands respectively (curve a). In curve 'b' and 'c' it has been observed that the increase of intensity of these bands at r-BSA1 and r-BSA2 revealed the structural reduction in protein and its increased content of carboxyl moieties [35,36]. The wide band observed at 3440 cm^{-1} (O–H stretch) in r-BSA2 and r-BSA1 as compared to pure BSA also affirms the creation of –OH groups due to reduction process. In SnO_2/SnS_2@r-BSA2 (curve e), the band became sharper and shifted from 3420 to 3470 cm^{-1}, decrease in intensity of protein main characteristic peaks, confirm the strong adsorption of SnO_2/SnS_2 QDs with r-BSA2. The same hypothesis was further supported and explained by Raman spectroscopy analysis (Fig. S2).

The surface morphologies of the as-synthesized r-BSA1, r-BSA2, SnO_2/SnS_2 QDs and SnO_2/SnS_2@r-BSA2 nanobiocomposite were characterized by FE-SEM. Fig. 2A shows the images of micro sized r-BSA1 in crystalline with micro pores which confirms the reduced structure. In this, we evidenced the little bit of aggregation at acidic pH condition (pH 3) due to the influence of disulfide bond integrity. After structural modification using reducing agent, structural change in r-BSA2 was observed in the form of microcapsules, reveal the cleavage of certain protein disulfide bonds in protein structure at circumneutral pH 7.2 (Fig. 2B). In Fig. 2C, found agglomerated form of SnO_2/SnS_2 QDs and their presence of elemental composition such as tin, oxygen, and sulfur was supported and tabulated in Fig. S3. Surprisingly as seen in Fig. 2D, the SnO_2/SnS_2 QDs decorated onto the r-BSA2 microcapsules shows a linear separation of QDs which is free from agglomeration in

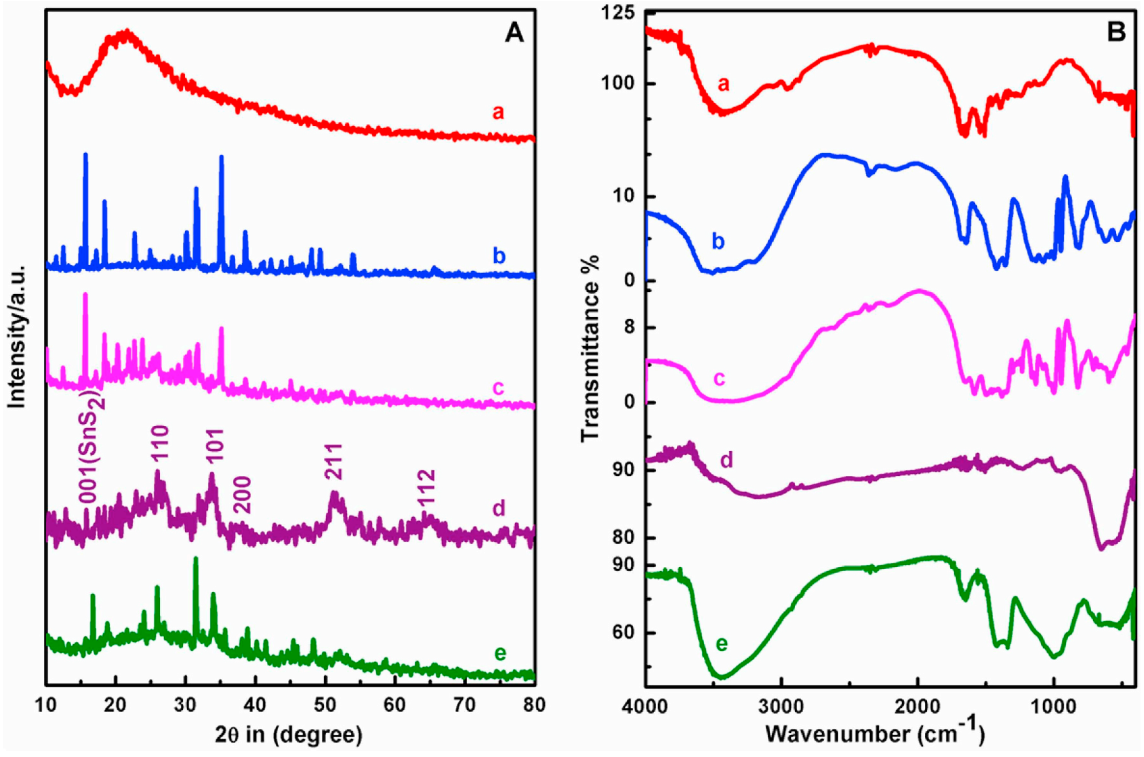

Fig. 1. (A) XRD patterns and (B) FT-IR spectrum of (a) BSA, (b) r-BSA1, (c) r-BSA2, (d) SnO_2/SnS_2 QDs, (e) SnO_2/SnS_2@r-BSA2 samples.

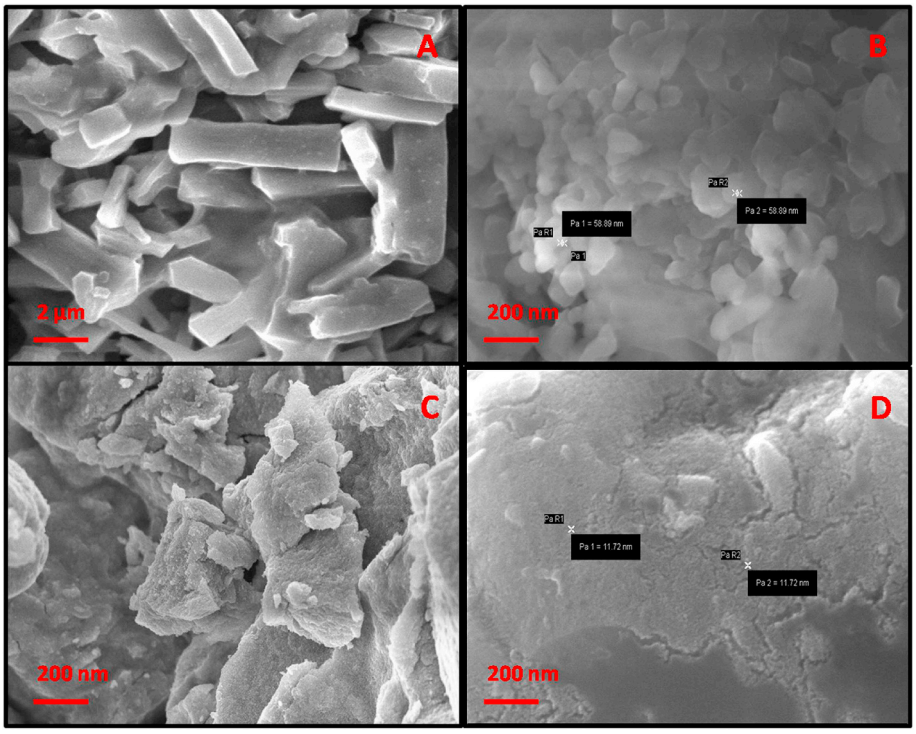

Fig. 2. SEM images of (A) r-BSA1, (B) r-BSA2, (C) SnO_2/SnS_2 QDs, (D) SnO_2/SnS_2@r-BSA2 nanobiocomposite.

composite, due to hydrophobic force and new functional groups such as –OH, –COOH, thiol groups developed between r-BSA2 and SnO_2/SnS_2 QDs. Moreover electrostatic attachment due to the interaction of sulfide group in SnO_2/SnS_2 QDs and positively charged lysine amino acid groups in protein microcapsules is also responsible to control the agglomeration. Therefore the biofuntionalization of SnO_2/SnS_2 QDs with r-BSA2 microcapsules results an exfoliated structure with large adhesive interfaces and diminished aggregation. The dispersible property of the prepared nanobiocomposite revealed remarkable ability of r-BSA2 in adsorption with SnO_2/SnS_2 QDs due to electrostatic and hydrophobic interactions (Fig. S4).

The surface elemental chemistry of as-prepared r-BSA2, SnO_2/SnS_2 QDs and SnO_2/SnS_2@r-BSA2 samples was further analyzed using XPS. From the survey XPS spectra (Fig. 3A), C1s, N1s, O1s and different valence spectra of Sn in individual sample and nanocomposite are evidenced. In Fig. 3B, r-BSA2 and SnO_2/SnS_2@r-BSA2 samples shows several C 1s peaks at 284.6 eV (C–C/C–H), 285.9 eV (aliphatic carbons of amino acid groups), 286.8 eV (NH-CHR-CO in protein backbone) and 288.4 eV (-CO-NH- peptidic carbons) [37]. The presence of these main peaks for protein in SnO_2/SnS_2@r-BSA2 evidenced the consistency of r-BSA2 after composite formation. The N1s peak recorded near 399.1 eV confirmed nitrogen in protein organic matrix and the decrease in concentration of N1s in SnO_2/SnS_2@r-BSA2 speculated the interaction of SnO_2/SnS_2 QDs with amino acid residues in protein (Fig. 3C). The broadening and red-shifted peak in SnO_2/SnS_2@r-BSA2 as compared to individual r-BSA2 affirmed the chemical interaction in composite formation [38]. Fig. 3D shows the narrow scan XPS spectra of O 1s electron orbital of the as-prepared samples, the increase in intensity of oxygen in SnO_2/SnS_2@r-BSA2 evidenced the raised oxygen groups on surface. It can be seen that in Fig. 3E, the two symmetrical peaks at 494.9 eV and 486.5 eV attributed to Sn $3d_{3/2}$ and Sn $3d_{5/2}$ respectively, and evidenced the presence Sn^{4+} which corresponds to SnS_2 and SnO_2 formation. The peak to peak separation of Sn $3d_{3/2}$ and Sn $3d_{5/2}$ is 8.4 eV which is in good agreement with reported SnO_2 spectrum [39] and presence of Sn^{4+} peaks in SnO_2/SnS_2@r-BSA2 attributed the chemical adsorption in composite. In Fig. 3F, revealed the deconvoluted peaks at 162.6, 162.89 and 163.8, 164.2 correspond to elemental sulfur. The increase in sulfur of SnO_2/SnS_2@r-BSA2 confirms the accumulation of thiol groups from r-BSA2 with SnO_2/SnS_2 QDs.

As can be seen from Fig. 4(A, B & D), the TEM images of r-BSA2 further supports the microcapsule morphology formation with corresponding SAED pattern. In Fig. 4(D &E) indexed the aggregated form of SnO_2/SnS_2 QDs with average particle size and standard deviation of 2.64 nm and 1.09 nm respectively (Fig. S5). The corresponding interspacing for SnO_2 and SnS_2 measured as 0.311 nm and 0.314 nm which are in agreement with the results of XRD pattern. In SAED pattern, it is further evidenced the formation of SnO_2/SnS_2 QDs with six diffraction rings, which corresponds to (001) plane of the hexagonal phase SnS_2 and (110), (101), (200), (211), (112) plane of the tetragonal phase of SnO_2 (Fig. 4F). Interestingly in Fig. 4(G and H), the well distributed form of SnO_2/SnS_2 QDs were observed due to the electrosteric forces from amino acid groups of r-BSA2 and their corresponding SAED pattern also further confirms the prepared nanobiocomposite (Fig. 4I). Here the calculated average particle size and standard deviation are 1.46 nm and 0.46 nm which also affirmed the avoidance of agglomeration in SnO_2/SnS_2 QDs with r-BSA2 microcapsules (Fig. S5).

This hypothesis further gets confirmed by UV–vis absorption spectra of BSA, r-BSA1, r-BSA2, SnO_2/SnS_2 QDs and SnO_2/SnS_2@r-BSA2 samples (Fig. 5A). The absorption peaks around 280 nm corresponds to π-π^* transition of aromatic amino acids and residues in pure BSA. Therefore the decrease in absorbance of r-BSA1 and r-BSA2 evidenced the cleavage of disulfide bond linkages in appropriate range, and thus support the size modification. In SnO_2/SnS_2, the smaller value of absorption peak reported to have smaller size of nanoparticles [40]. Herein, the decrease in absorption peak value of SnO_2/SnS_2@r-BSA2 represents the avoidance of agglomeration in SnO_2/SnS_2 QDs due to steric attachment of r-BSA2.

Magnetic measurements of SnO_2/SnS_2 QDs, r-BSA2 and SnO_2/SnS_2@r-BSA2 nanobiocomposite (Fig. 5B) observed negative magnetic moment denoted diamagnetic nature with saturation magnetization (M_s) of 6.766×10^{-4}, 4.144×10^{-4}, 0.476×10^{-4} emu/g. The decrease in M_s value indicates the grain size reduction when compared to bulk material [41]. Here, we found the reduction of M_s in SnO_2/SnS_2@/r-BSA2 as compared to SnO_2/SnS_2 QDs due to the increased adhesive

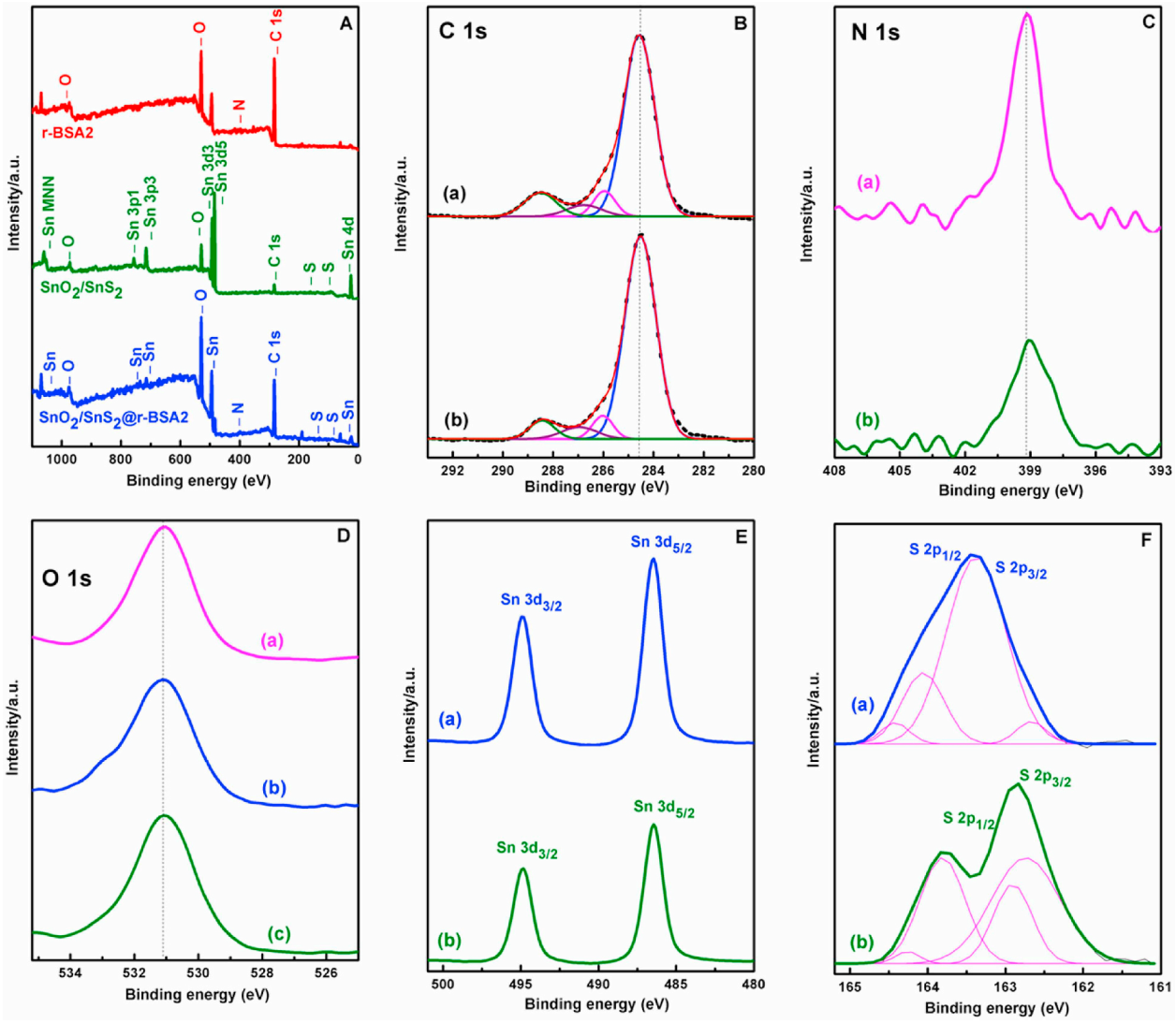

Fig. 3. (A) XPS survey spectra, High resolution XPS spectra of (B) Deconvoluted C1s and (C) N1s for (a) r-BSA2 and (b) SnO_2/SnS_2@r-BSA2, (D) O1s for (a) r-BSA2 (b) SnO_2/SnS_2 QDs and SnO_2/SnS_2@r-BSA2, (E) Sn3d and (F) Deconvoluted S2p of (a) SnO_2/SnS_2 QDs and (b)SnO_2/SnS_2@r-BSA2 samples.

surfaces in QDs.

3.2. Electrochemical behavior of the modified electrode in Mel detection

The effect of pH on the electrochemical behavior of 10 mM of Mel in 0.1 M of PBS at different pH ranges (1.0–10.0) for SnO_2/SnS_2@r-BSA2 nanobiocomposite was carefully studied. Fig. S6, shows the maximum oxidation peak current of Mel obtained at pH 7.0 and shown decreased oxidation peak current at other pH ranges. Therefore, PBS with pH 7.0 was selected as supporting electrolyte for resulting best sensitivity in all subsequent electrochemical studies. In addition the oxidation peak potential of Mel shifts negatively with an increase in pH due to the effective involvement of protons in electrode reaction process. The electrochemical behavior of 200 μM Mel for bare, BSA, r-BSA1, r-BSA2, SnO_2/SnS_2 QDs, SnO_2/SnS_2@r-BSA2 modified Glassy caron electrode (SnO_2/SnS_2@r-BSA2/GCE) were studied by Cyclic voltammetry (CV) in 0.1 M of PBS and reported in Fig. 6A. It can be observed that the oxidation peak current for SnO_2/SnS_2@r-BSA2/GCE has increased, compared to other modified electrodes in which the electrosteric stabilization of SnO_2/SnS_2 QDs by r-BSA2 on electrode surface facilitate more surface area eventually causing significant change in electrocatalytic behavior towards Mel. Furthermore, the oxidation peak potential of SnO_2/SnS_2 QDs, r-BSA2 and SnO_2/SnS_2@r-BSA2/GCE was found as 0.728 V, 0.705 V and 0.691 V respectively. It is saying that the SnO_2/SnS_2@r-BSA2/GCE resulted not only the increased sensitivity but also a low oxidation potential in Mel sensing as compared to individual material modified electrodes, ascribed its promising electroanaytical behavior. To understand the better adsorption behavior of r-BSA2 with SnO_2/SnS_2 QDs, the prepared nanobiocomposite of SnO_2/SnS_2@r-BSA2 has been compared with the SnO_2 QDs decorated r-BSA2 (SnO_2@r-BSA2) and SnS_2 QDs decorated r-BSA2 (SnS_2@r-BSA2) samples as in Fig. S7. In that, it was observed higher sensitivity with oxidation peak potential of 0.68 V towards Mel for SnO_2/SnS_2@r-BSA2 modified SPE (SnO_2/SnS_2@r-BSA2/SPE) attributed to the raised surface binding sites in SnO_2/SnS_2 QDs nanocomposite with r-BSA2 as compared to SnO_2@r-BSA2/SPE and SnS_2@r-BSA2/SPE. The effect of scan rate on electrochemical behavior of 100 μM Mel for the SnO_2/SnS_2@r-BSA2/SPE was investigated in 0.1 M PBS and plotted in Fig. 6B. As increase in scan rate, a gradual increase in oxidation peak currents of Mel is noticed and found linear relationship between peak current and square root of scan rate in the range of 10–100 mV s^{-1} with linear equation $y = 14.1337x + 0.8860$ and $R^2 = 0.9958$. This study supports the diffusion controlled phenomena of SnO_2/SnS_2@r-BSA2/SPE.

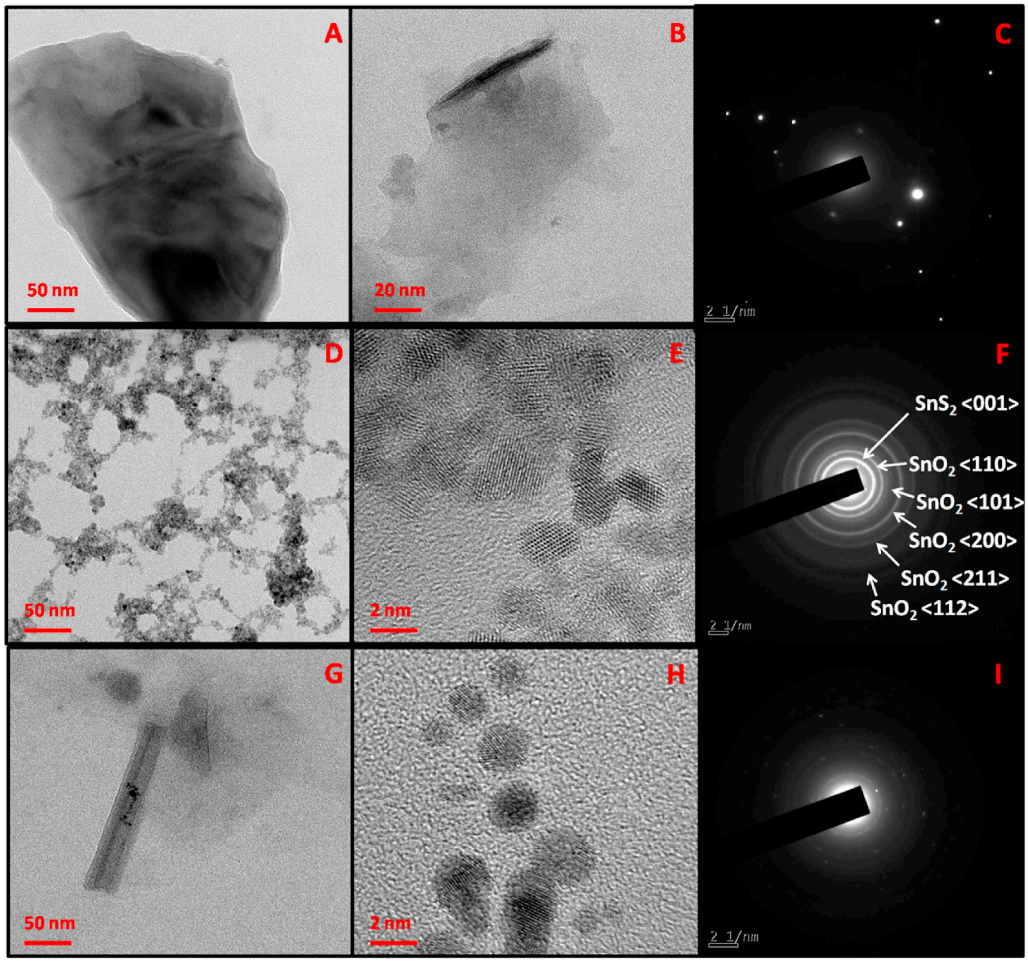

Fig. 4. TEM, HR-TEM images and SAED pattern of (A, B & C) r-BSA2, (D, E & F) SnO_2/SnS_2 QDs, (G, H & I) SnO_2/SnS_2@r-BSA2 samples.

3.3. Nonenzymatic electrocatalytic detection of Mel

Under the optimized condition, the determination of Mel at SnO_2/SnS_2@r-BSA2 nanobiocomposite modified electrode was carried out in 0.1 M PBS (pH 7.0) by Square Wave Voltammetry (SWV) and the results are illustrated in Fig. 7. It can seen that the increasing concentration of Mel results linearly increase in SWV anodic peak currents with lower detection limit of 16 nM (S/N = 3σ) and linear range of 0.2–1000 μM. The first linear dynamic range was from 0.2 μM to 1 μM, with a calibration equation of $I_p(\mu A) = 0.2178 + 0.2643C$ (μM) (R = 0.9996) and the second linear dynamic range was from 2 μM to 20 μM, with a calibration equation of $I_p(\mu A) = 1.0323 + 0.4326C$ (μM) (R = 0.9989). The raised –OH groups, –COOH and thiol groups accumulated from both r-BSA2 and SnO_2/SnS_2 QDs responsible for electrostatic/covalent interaction towards –NH groups in Mel, whereas the positively charged residues in r-BSA2 provide strong electrostatic and hydrophobic interaction towards SnO_2/SnS_2 QDs. Thus, the increased synergistic effect in the prepared hybrid nanobiocompsite enhanced the

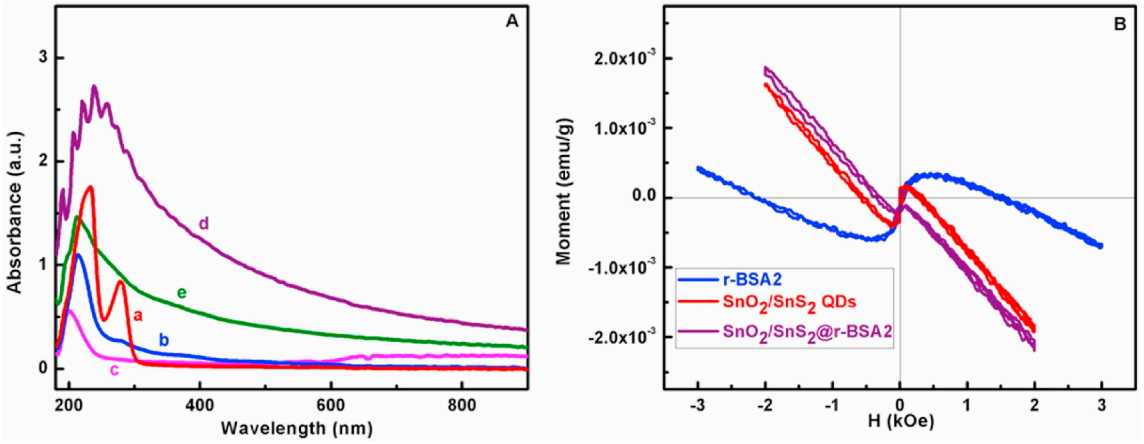

Fig. 5. (A) UV–vis spectra of (a) BSA, (b) r-BSA1, (c) r-BSA2, (d) SnO_2/SnS_2 QDs, (e) SnO_2/SnS_2@r-BSA2 nanobiocomposite and (B) VSM analysis of prepared samples.

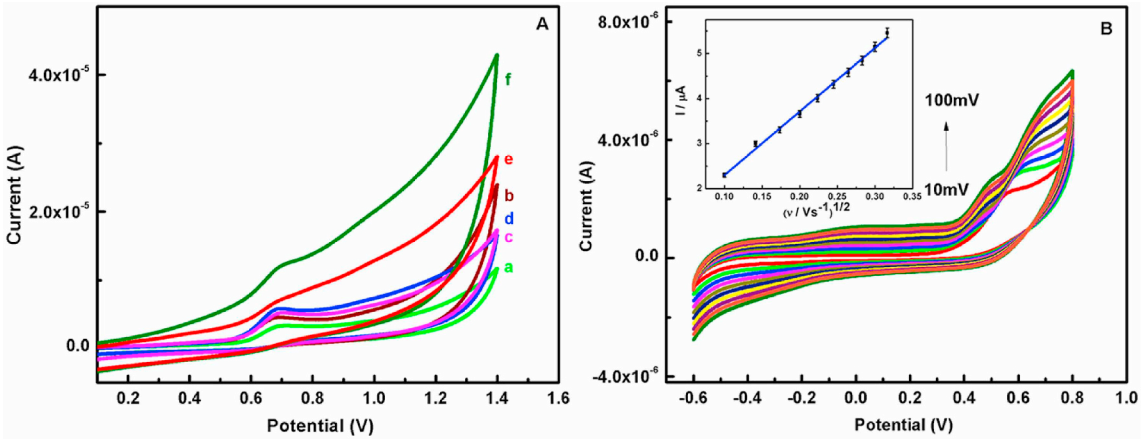

Fig. 6. (A) CVs obtained for 200 μM of Mel at the (a) bare, (b) BSA, (c) r-BSA1, (d) r-BSA2, (e) SnO_2/SnS_2 QDs, (d) SnO_2/SnS_2@r-BSA2 modified GCE in 0.1 M PBS at a scan rate of 50 mV s^{-1} (pH7). (B) Effect of scan rate on the electrochemical behavior of SnO_2/SnS_2@r-BSA2/SPE in the presence of 100 μM of Mel in 0.1 M PBS at pH7 and inset Fig. shows the corresponding linear fit for anodic oxidation peak current vs. square root of scan rate.

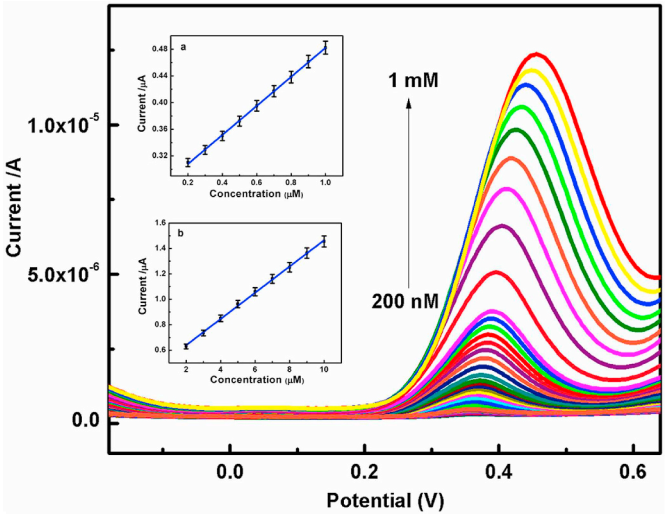

Fig. 7. SWV of Mel sensing for SnO_2/SnS_2@r-BSA2/SPE in 0.1 M PBS at pH7. Inset Fig. shows the corresponding linear fit from (a) 0.2–1 μM, (b) 2–10 μM of Mel concentration.

selective determination towards Mel with better stability. Table 1 shows comparison of prepared SnO_2/SnS_2@r-BSA2 with some of the reported hybrid composite modified electrodes for Mel sensing and found that the as-synthesized nanobiocomposite exhibits a satisfactory performance with low detection limit and wide linear range than other reports.

3.4. Stability, reproducibility, anti-interference property and real sample detection of SnO_2/SnS_2@r-BSA2/SPE

The better selectivity of sensing of Mel among other potential interfering species ensures high accuracy of measurement by the prepared SnO_2/SnS_2@r-BSA2/SPE. Herein, the interference test was carried out under optimum conditions using chronoamperometry technique by successive addition of 20 μM of Mel and 200 μM of each potential interefering species such as Ascorbic acid (AA), Uric acid (UA), Hydroxylamine hydrochloride (HA), L-Tyrosine (Tyr), Dopamine (DA), Riboflavin (RF), Acetylcholine (ACh), L-Arginine (L-Arg), L-Glutamic acid (L-GA), Folic acid (FA) at the applied potential of 0.68 V (Fig. 8A). It is observed that the addition of 20 μM Mel resulted in significant and quick current response, while addition of interfering species caused negligible current changes. The oxidation peak potential for individual interfering species was studied using CV and observed feeble current change at potential values of −0.02 V, 0.13 V, 0.74 V, 0.5 V, 0.08 V, −0.25 V, −0.4 V, −0.22 V, 0.31 V and 0.75 V for AA, UA, HA, Tyr, DA, RF, ACh, L-Arg, L-GA and FA respectively (Fig. S8). Thus SnO_2/SnS_2@r-BSA2/SPE was highly selective towards the determination of Mel even in the presence of interfering compounds with high concentration. The stability of the SnO_2/SnS_2@r-BSA2 nanobiocomposite

Table 1
Performance of different modified electrodes in sensing of Mel.

S. No	Electrode	Detection Method	Detection Limit (μM)	Linear Range (μM)	Ref.
1	ZnO/3,4′AAZ/CPE	SWV	0.056	0.3–100	[24]
2	AHNSA:PdNPs:ErGO/GCE	SWV	0.09	5–100	[25]
3	Boron doped diamond electrode	SWV	0.6	4.3–430	[42]
4	Graphene oxide/SPE	DPV	1.1	5–3000	[43]
5	Graphene/SPE	Amperometry	0.87	–	[44]
6	RGO/RuO_2/GCE	DPV	0.18	2–20	[45]
7	MnHCF-PEDOT/GCE	Amperometry	10	100–4600	[46]
8	Boron doped diamond electrode	DPV	10.3	344.4–688.8	[47]
9	MWCNTs/DHP/GCE	LSV	0.02	0.082–10	[48]
10	Activated GCE	LSV	0.05	0.8–100	[49]
11	Boron doped diamond electrode	DPV	0.11	0.5–4	[50]
12	SnO_2/SnS_2@r-BSA2/SPE	SWV	0.016	0.2–1000	this work

AHNSA:PdNPs:ErGO/GCE: 4-amino-3-hdroxy-1-naphthalene sulfonic acid, PdNPs: palladium nanoparticle, ErGO: Electrochemically reduced Graphene Oxide, ZnO: Zinc Oxide, 3,4′AAZ: 3-(4′-amino-3′-hydroxy-biphenyl-4-yl)-acrylic acid, CPE: Carbon paste electrode, SPE: Screen Printing Electrode, RGO: Reduced Graphene Oxide, RuO_2: Ruthenium Oxide, MnHCF: Manganese hexacyanoferrate, PEDOT: poly(3, 4-ethylenedioxythiophene), MWCNTs: Multiwalled Carbon Nanotubes, DHP: dihexadecyl hydrogen phosphate.

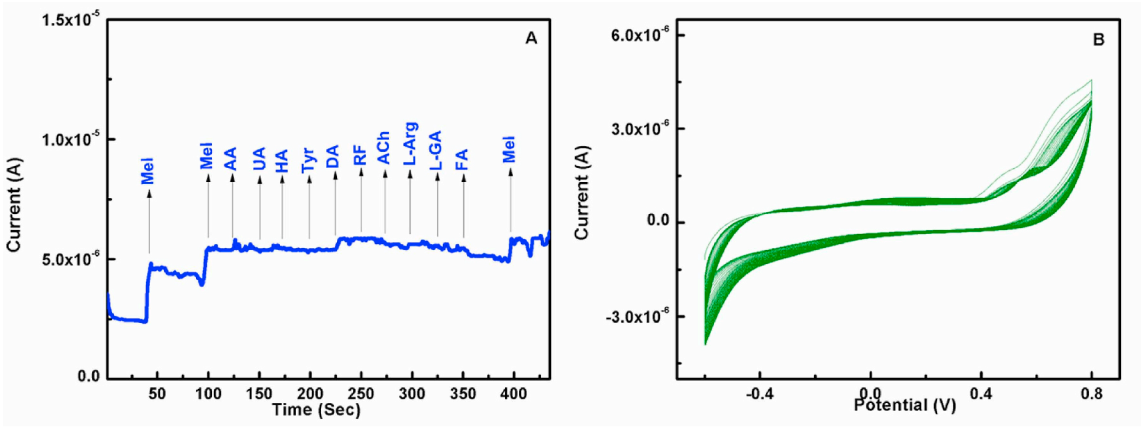

Fig. 8. (A) Amperometric study of Mel for SnO_2/SnS_2@r-BSA2/SPE in 0.1 M PBS (pH7) at applied potential of 0.68 V. (B) Stability study of SnO_2/SnS_2@r-BSA2/SPE at 50 cylcles with 100 μM of Mel in 0.1 M PBS at scan rate of 50 mV s^{-1} and pH7.

was studied in CV of 50 cycles with 100 μM of Mel in 0.1 M PBS and shown in Fig. 8B.

The reproducibility of the prepared SnO_2/SnS_2@r-BSA2/SPE was further evaluated by employing five nanobiocomposite modified electrodes for the detection of 50 μM Mel in similar conditions such as 0.1 M PBS (pH 7.0) using SWV (Fig. 9A). The calibrated histogram is shown in the inset Fig. 9A and their corresponding RSD 1.17% was calculated. Additionally, the long-term stability of the prepared SnO_2/SnS_2@r-BSA2/SPE was also assessed by storing modified electrode at 5 °C and employed for the detection of 60 μM by SWV (Fig. 9B) in consecutive 10 days. The corresponding calibrated histogram was shown in inset Fig. 9B and revealed good stability with least decrease in current sensitivity around ~4% after 10 days of evaluation. To validate the proposed analysis method, the detection of Mel content in urine samples from 3 healthy volunteers were carried out. Then the collected urine samples were diluted twice with PBS (pH 7.0) and spiked with 50 μM of Mel. The concentration of Mel in 3 different samples were found with satisfactory recovery and listed in Table 2. Therefore, it was evident that the proposed SnO_2/SnS_2@r-BSA2/SPE could be successfully applied for the selective determination of Mel for biomedical application.

Table 2
Determination of Mel in human urine samples.

Samples	Added (μM/L)	Total found (μM/L)	% of recovery	RSD%
sample 1	50	53.4 ± 0.3	106.8	1.5
sample 2	50	50.5 ± 0.2	101.0	1.9
sample 3	50	48.2 ± 0.4	96.4	1.6

4. Conclusions

In summary, we have developed a novel nanobiocomposite comprising of SnO_2/SnS_2 QDs adsorbed r-BSA2 protein microcapsules as sensing template for Mel detection. In addition, the structural amendments of BSA at different pH conditions and its steric interaction with SnO_2/SnS_2 QDs were extensively investigated. Interestingly, the fabricated nanobiocomposite exhibited a diamagnetic behavior with increased grain size and accumulated active sites upon composite formation, enabled friendly interface for the efficient conjugation towards Mel. The constructed electrocatalytic SnO2/SnS2@r-BSA2 biosensor exhibited high sensitivity, selectivity and stability for the selective determination of Mel with lowest detection limit of 16 nM. Moreover, the proposed biosensor manifested reduced oxidation potential (0.68 V) in Mel sensing and thus facilitates the improvised electroanalytical performance. In addition, the recovery of Mel concentration in real sample also conceptually supports the versatile performance of the fabricated enzyme free biosensor in real-time practical application.

Notes

The authors declare no competing financial interest.

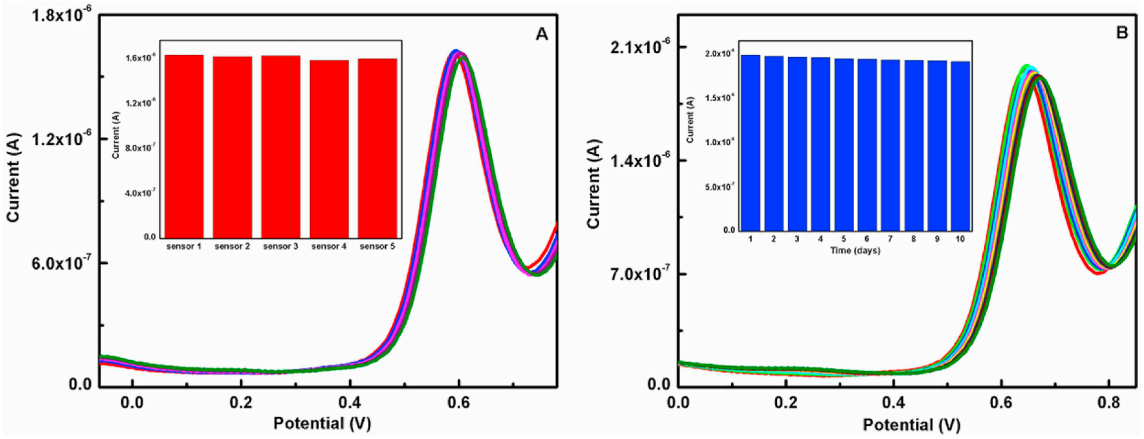

Fig. 9. Reproducibility and long-term stability measurements. (A) SWV response of five SnO_2/SnS_2@r-BSA2/SPE prepared in similar conditions for the detection of 50 μM Mel in 0.1 M PBS solution (pH7). Inset shows the calibrated histogram; (B) the SWV response of SnO_2/SnS_2@r-BSA2/SPE for the detection of 60 μM Mel in 0.1 M PBS solution (pH7) for ten days. Inset shows the calibrated histogram of stability test.

Declaration of competing interests

The authors declare that they have no known competing financial interests or personal relationships that could have appeared to influence the work reported in this paper.

Acknowledgements

This work was financially supported by Science & Engineering Research Board (EMR/2014/000010) and RUSA 2.0 [F.24–51/2014-U, Policy (TN Multi-Gen), Dept of Edn, Gol] for financial assistance. FE-SEM, EDX, TEM and XPS characterization was carried out at the IITBNF, IITB under INUP which is sponsored by MeitY, Government of India.

Appendix A. Supplementary data

Supplementary data to this article can be found online at https://doi.org/10.1016/j.talanta.2019.120671.

References

[1] S. Bhuiya, A.B. Pradhan, L. Haque, S. Das, Molecular aspects of the interaction of iminium and alkanolamine forms of the anticancer alkaloid chelerythrine with plasma protein bovine serum albumin, J. Phys. Chem. B 120 (2016) 5–17.
[2] Q. Liu, H. Zhu, J. Qin, H. Dong, J. Du, Theranostic vesicles based on bovine serum albumin and poly(ethylene glycol)-*block*-poly(l-lactic-*co*-glycolic acid) for magnetic resonance imaging and anticancer drug delivery, Biomacromolecules 15 (2014) 1586–1592.
[3] M. Yang, C. Dutta, A. Tiwari, Disulfide-bond scrambling promotes amorphous aggregates in lysozyme and bovine serum albumin, J. Phys. Chem. B 119 (2015) 3969–3981.
[4] K. Kubiak-Ossowska, K. Tokarczyk, B. Jachimska, P.A. Mulheran, Bovine serum albumin adsorption at a silica surface explored by simulation and experiment, J. Phys. Chem. B 121 (2017) 3975–3986.
[5] B.E. Givens, Z. Xu, J. Fiegel, V.H. Grassian, Bovine serum albumin adsorption on SiO_2 and TiO_2 nanoparticle surfaces at circumneutral and acidic pH: a tale of Two Nano-bio Surface Interactions, J. Colloid Interface Sci. 493 (2017) 334–341.
[6] Z. Li, T. Yang, C. Lin, Q. Li, S. Liu, F. Xu, H. Wang, X. Cui, Sonochemical synthesis of hydrophilic drug loaded multifunctional bovine serum albumin nanocapsules, ACS Appl. Mater. Interfaces 7 (2015) 19390–19397.
[7] S. Alam, A. Mukhopadhyay, Conjugation of gold nanorods with bovine serum albumin protein, J. Phys. Chem. C 118 (2014) 27459–27464.
[8] P. Du, J. Zhao, H. Mashayekhi, B. Xing, Adsorption of bovine serum albumin and lysozyme on functionalized carbon nanotubes, J. Phys. Chem. C 118 (2014) 22249–22257.
[9] M.A. Dobreva, R.J. Green, I. Mueller-Harvey, J.-P. Salminen, B.J. Howlin, R.A. Frazier, Size and molecular flexibility affect the binding of ellagitannins to bovine serum albumin, J. Agric. Food Chem. 62 (2014) 9186–9194.
[10] S. Mondal, C. Li, K. Wang, Bovine serum albumin adsorption on gluteraldehyde cross-linked chitosan hydrogels, J. Chem. Eng. Data 60 (2015) 2356–2362.
[11] Y. Zhou, Y. Bai, H. Liu, X. Jiang, T. Tong, L. Fang, D. Wang, Q. Ke, J. Liang, S. Xiao, Tellurium/Bovine serum albumin nanocomposites induce the formation of stress granules in a protein kinase R dependent manner, ACS Appl. Mater. Interfaces 10 (2018) 25241–25251.
[12] S. Xia, Y. Li, Q. Zhao, J. Li, Q. Xia, X. Zhang, Q. Huang, Probing conformational change of bovine serum albumin – dextran conjugates under controlled dry heating, J. Agric. Food Chem. 63 (2015) 4080–4086.
[13] A. Akkouch, G. Shi, Z. Zhang, M. Rouabhia, Bioactivating electrically conducting polypyrrole with fibronectin and bovine serum albumin, J. Biomed. Mater. Res. 92A (2009) 221–231.
[14] K.M. Au, S.P. Armes, Heterocoagulation as a facile route to prepare stable serum albumin-nanoparticle conjugates for biomedical applications: synthetic protocols and mechanistic insights, ACS Nano 6 (2012) 8261–8279.
[15] F. Xu, S. Ren, Y. Gu, A novel conductive poly(3,4-ethylenedioxythiophene)-BSA film for the construction of a durable HRP biosensor modified with nano Au particles, Sensors 16 (2016) 374–384.
[16] J. Jin, Z. Huang, G. Yin, J. Lin, Q. Li, D. Han, Preparation of polypyrrole-protein composite films and the electrochemically controlled release of proteins, J. Nanosci. Nanotechnol. 16 (2016) 2283–2290.
[17] R. Cui, H.C. Pan, J.J. Zhu, H.Y. Chen, Versatile immunosensor using CdTe quantum dots as electrochemical and fluorescent labels, Anal. Chem. 79 (2007) 8494–8501.
[18] Y. Xu, J. Liang, C. Hu, F. Wang, S. Hu, Z. He, A hydrogen peroxide biosensor based on the direct electrochemistry of hemoglobin modified with quantum dots, J. Biol. Inorg. Chem. 12 (2007) 421–427.
[19] D. Du, S. Chen, D. Song, H. Li, X. Chen, Development of acetylcholinesterase biosensor based on CdTe quantum dots/gold nanoparticles modified chitosan microspheres interface, Biosens. Bioelectron. 24 (2008) 475–479.
[20] Y.C. Zhang, Z.N. Du, K.W. Li, M. Zhang, Size-controlled hydrothermal synthesis of SnS_2 nanoparticles with high performance in visible light-driven photocatalytic degradation of aqueous methyl orange, Separ. Purif. Technol. 81 (2011) 101–107.
[21] Y. Shiga, N. Umezawa, N. Srinivasan, S. Koyasu, E. Sakai, M. Miyauchi, A metal sulfide photocatalyst composed of ubiquitous elements for solar hydrogen production, Chem. Commun. 52 (2016) 7470–7473.
[22] D.H. Youn, S.K. Stauffer, P. Xiao, H. Park, Y. Nam, A.D. Dolocan, G. Henkelman, A. Heller, C.B. Mullins, Simple synthesis of nanocrystalline tin sulfide/N-doped reduced graphene oxide composites as lithium ion battery anodes, ACS Nano 10 (2016) 10778–10788.
[23] P. Cai, D.K. Ma, Q.C. Liu, S.M. Zhou, W. Chen, S.M. Huang, Conversion of ternary Zn_2SnO_4 octahedrons into binary mesoporous SnO_2 and hollow SnS_2 hierarchical octahedrons by template-mediated selective complex extraction, J. Mater. Chem. A 1 (2013) 5217–5223.
[24] C.R. Patra, A. Odani, V.G. Pol, D. Aurbach, A. Gedanken, Microwave-assisted synthesis of tin sulfide nanoflakes and their electrochemical performance as Li-inserting materials, J. Solid State Electrochem. 11 (2007) 186–194.
[25] C.H. Lai, M.Y. Lu, L.J. Chen, Metal sulfide nanostructures: synthesis, properties and applications in energy conversion and storage, J. Mater. Chem. 22 (2012) 19–30.
[26] E. Molaakbari, A. Mostafavi, H. Beitollahi, Simultaneous electrochemical determination of dopamine, melatonin, methionine and caffeine, Sens. Actuators B Chem. 208 (2015) 195–203.
[27] N. Kumar, Rosy, R.N. Goyal, Nanopalladium grained polymer nanocomposite based sensor for the sensitive determination of melatonin, Electrochim. Acta 211 (2016) 18–26.
[28] I. Reinholds, I. Pugajeva, V. Radenkovs, J. Rjabova, V. Bartkevics, Development and validation of new ultra-high-performance liquid chromatography–hybrid quadrupole-orbitrap mass spectrometry method for determination of melatonin in fruits, J. Chromatogr. Sci. 54 (2016) 977–984.
[29] A.A. Vitale, C.C. Ferrari, H. Aldana, J.M. Affanni, Highly sensitive method for the determination of melatonin by normal-phase high performance liquid chromatography with fluorometric detection, J. Chromatogr. B Biomed. Sci. Appl. 681 (1996) 381–384.
[30] E. Oladi, M. Mohamadi, T. Shamspur, A. Mostafavi, Spectrofluorimetric determination of melatonin in kernels of four different pistacia varieties after ultrasound-assisted solid–liquid extraction, Spectrochim. Acta A 132 (2014) 326–329.
[31] A.S. Amin, M. Zaky, A.M. El-Beshbeshy, Colorimetric estimation of melatonin in pharmaceutical formulations, Microchim. Acta 135 (2000) 81–85.
[32] D. Chen, L. Gao, Novel synthesis of well-dispersed crystalline SnO_2 nanoparticles by water-in-oil microemulsion-assisted hydrothermal process, J. Colloid Interface Sci. 279 (2004) 137–142.
[33] Y. Liu, P. Chen, Y. Chen, H. Lu, J. Wang, Z. Yang, Z. Lu, M. Li, L. Fang, In situ ion-exchange synthesis of SnS_2/g-C_3N_4 nanosheets heterojunction for enhancing photocatalytic activity, RSC Adv. 6 (2016) 10802–10809.
[34] S. Yan, K. Li, Z. Lin, H. Song, T. Jiang, J. Wu, Y. Shi, Fabrication of a reversible SnS_2/RGO nanocomposite for high performance lithium storage, RSC Adv. 6 (2016) 32414–32421.
[35] T.S. Anirudhan, A.R. Tharun, S.R. Rejeena, Investigation on poly(methacrylic acid)-grafted cellulose/bentonite superabsorbent composite: synthesis, characterization, and adsorption characteristics of bovine serum albumin, Ind. Eng. Chem. Res. 50 (2011) 1866–1874.
[36] D. Nathiya, J. Wilson, K. Gurunathan, Interactive studies on synthetic nanopolymer decorated with edible biopolymer and its electrochemical biosensing application, Sci. Rep. 9 (2019) 1–12.
[37] E. Vanea, V. Simon, XPS study of protein adsorption onto nanocrystalline aluminosilicate microparticles, Appl. Surf. Sci. 257 (2011) 2346–2352.
[38] J.J. Won, R. Nirmala, R. Navamathavan, H.Y. Kim, Electrospun core–shell nanofibers from homogeneous solution of poly(vinyl alcohol)/bovine serum albumin, Int. J. Biol. Macromol. 50 (2012) 1292–1298.
[39] H. Feng, C. Li, T. Li, F. Diao, T. Xin, B. Liu, Y. Wang, Three-dimensional hierarchical SnO_2 dodecahedral nanocrystals with enhanced humidity sensing properties, Sens. Actuators B Chem. 243 (2017) 704–714.
[40] M. Salavati-Niasari, D. Ghanbari, F. Davar, Shape selective hydrothermal synthesis of tin sulfide nanoflowers based on nanosheets in the presence of thioglycolic acid, J. Alloy. Comp. 492 (2010) 570–575.
[41] R.D. Zysler, E. Lima Jr., M. Vasquez Mansilla, H.E. Troiani, M.L. Mojica Pisciotti, P. Gurman, A. Lamagna, L. Colombo, A new quantitative method to determine the uptake of SPIONs in animal tissue and its application to determine the quantity of NPs in the liver and lung of balb-c mice exposed to the SPIONs, J. Biomed. Nanotechnol. 9 (2013) 1–4.
[42] N. Alpar, P.T. Pınar, Y. Yardım, Z. Şentürk, Voltammetric method for the simultaneous determination of melatonin and pyridoxine in dietary supplements using a cathodically pretreated boron-doped diamond electrode, Electroanalysis 29 (2017) 1691–1699.
[43] F.J.V. Gomez, A. Martín, M.F. Silva, A. Escarpa, Screen-printed electrodes modified with carbon nanotubes or graphene for simultaneous determination of melatonin and serotonin, Microchim. Acta 182 (2015) 1925–1931.
[44] I.M. Apetrei, C. Apetrei, Voltammetric determination of melatonin using a graphene-based sensor in pharmaceutical products, Int. J. Nanomed. 11 (2016)

1859–1866.
[45] B. Devadas, R. Madhu, S.M. Chen, V. Veeramani, M. Rajkumar, Electrochemical preparation of a reduced graphene oxide/ruthenium oxide modified electrode and its application to the simultaneous determination of serotonin and melatonin, Sci. Adv. Mater. 7 (2015) 654–662.
[46] T.H. Tsai, Y.C. Huang, S.M. Chen, Manganese hexacyanoferrate with poly (3, 4-ethylenedioxythiophene) hybrid film modified electrode for the determination of catechin and melatonin, Int. J. Electrochem. Sci. 6 (2011) 3238–3253.
[47] A.T. Ball, B.A. Patel, Rapid voltammetric monitoring of melatonin in the presence of tablet excipients, Electrochim. Acta 83 (2012) 196–201.
[48] W. Qu, F. Wang, S. Hu, D. Cui, Electrocatalytic properties and voltammetric determination of melatonin at a nanostructured film electrode, Microchim. Acta 150 (2005) 109–114.
[49] W. Xiao-Ping, Z. Lan, L. Wen-Rong, D. Jian-Ping, C. Hong-Qing, C. Guo-Nan, Study on the electrochemical behavior of melatonin with an activated electrode, Electroanalysis 14 (2002) 1654–1660.
[50] A. Levent, Electrochemical determination of melatonin hormone using a boron-doped diamond electrode, Diam. Relat. Mater. 21 (2012) 114–119.